

# Measurement report: Airborne Observation of CO<sub>2</sub> and CH<sub>4</sub> in the Urban Atmospheric Boundary Layer in Eastern China

Jun Wang<sup>1</sup>, Honghui Xu<sup>2</sup>, Wei Xiao<sup>1,3\*</sup>, Yuting Pang<sup>2</sup>, Ning Hu<sup>4</sup>, Jiaping Xu<sup>5</sup>, Yibo Liu<sup>4</sup>, Lingbing Bu<sup>4</sup>, Chang Cao<sup>1</sup>, Zhonghao Yang<sup>1</sup>, Tianhao Wang<sup>1</sup>, Lei Jia<sup>1</sup>, Jinhui Wu<sup>1</sup>, Mi Zhang<sup>1</sup>, Xuhui Lee<sup>6</sup>

5 <sup>1</sup> Yale-NUIST Center on Atmospheric Environment, Key Laboratory of Ecosystem Carbon Source and Sink, China Meteorological Administration, Nanjing University of Information Science and Technology, Nanjing, Jiangsu Province 210044, China

<sup>2</sup> Zhejiang Lin'an Atmospheric Background National Observation and Research Station, Zhejiang Institute of Meteorological Sciences, Hangzhou, Zhejiang Province 311300, China

10 <sup>3</sup> State Key laboratory of Climate System Prediction and Risk Management, Nanjing University of Information Science & Technology, Nanjing, Jiangsu Province 210044, China

<sup>4</sup> Collaborative Innovation Center on Forecast and Evaluation of Meteorological Disasters, Nanjing University of Information Science & Technology, Nanjing, Jiangsu Province 210044, China

<sup>5</sup> Jiangsu Climate Center, Nanjing, Jiangsu Province 210019, China

15 <sup>6</sup> School of the Environment, Yale University, New Haven, Connecticut 06511, USA

*Correspondence to:* Wei Xiao (wei.xiao@nuist.edu.cn)

**Abstract.** To characterize the concentrations of CO<sub>2</sub> and CH<sub>4</sub> in the urban atmospheric boundary layer (ABL), this study conducted airborne measurements over four cities in Eastern China, obtaining full vertical profiles (ground to 2 km) over Beijing and Nanjing, partial profiles over Hengshui and Shangqiu. Results showed that the CO<sub>2</sub> and CH<sub>4</sub> concentrations in the ABL were consistently higher than those in the free atmosphere, with the highest values observed near the surface (Beijing and Nanjing). In Beijing, the daytime and nighttime inversion jumps in the CO<sub>2</sub> concentration were  $-25.2 \pm 0.4$  ppm and  $-18.0 \pm 0.2$  ppm, respectively. In Nanjing, the corresponding values were  $-9.5 \pm 0.1$  ppm and  $-10.0 \pm 0.4$  ppm. For CH<sub>4</sub>, the inversion jumps were  $-171.4 \pm 0.4$  ppb during the day and  $-202.6 \pm 2.3$  ppb at night (Beijing); in Nanjing, they were  $-140.7 \pm 0.1$  ppb and  $-108.0 \pm 2.1$  ppb, respectively. Change in the air mass trajectory altered the free-atmospheric CO<sub>2</sub> concentration over Nanjing by 3 ppm in a matter of a few hours. The EDGAR CH<sub>4</sub>:CO<sub>2</sub> emissions ratio was within measurement uncertainty of the nighttime ABL value in Beijing, but about 80% higher in Nanjing, indicating that the inventory may have missed the recent energy transition from gasoline and natural gas to electric in the transport sector. The experimental data is available at <https://doi.org/10.7910/DVN/ZPVSUU>.

## 1 Introduction

30 This study is an experimental investigation of atmospheric CO<sub>2</sub> and CH<sub>4</sub> in the urban atmospheric boundary layer (ABL) in Eastern China. The ABL refers to the lowest layer of air between the Earth's surface and the free atmosphere, with a typical thickness of 1 km on land. Measurements of CO<sub>2</sub> and CH<sub>4</sub> in the ABL are motivated by several scientific considerations. Observational studies of the ABL structure are usually made with potential temperature and water vapor. These two scalars are typically conserved if in the ABL when it is free of clouds and aerosols. In polluted conditions or if clouds are present,

35 they are no longer conserved, which complicates the diagnostic analysis of the ABL depth and its time evolution (Lee, 2023).  
CO<sub>2</sub> and CH<sub>4</sub>, on the other hand, are conserved scalars in the clear, the cloudy and the polluted ABL when chemical destruction  
and generation are absent. Their presence does not affect air motion. Although they may participate in chemical reactions in  
the ABL, these reactions have no dynamic consequence at timescales relevant to ABL processes. In regions with heavy  
40 pollution, such as Eastern China and Northern India, it is advantageous to study the ABL dynamics with CO<sub>2</sub> and CH<sub>4</sub> profiles  
in addition to temperature and water vapor.

CO<sub>2</sub> and CH<sub>4</sub> concentrations in the ABL reveal information on surface-air exchanges at the landscape scale (10 – 100 km) (e.  
g., Denmead et al., 1996; Xueref-Remy et al., 2011). Their vertical profiles are often used in the ABL budget framework to  
determine the surface fluxes. A complete budget analysis requires observation or parameterization of the ABL depth, the time  
45 rate of change of the concentration, horizontal advection, and the entrainment flux at the ABL top (Crawford et al., 2016; Vilà-  
Guerau de Arellano et al., 2004; Trousdell et al., 2016). In situations where horizontal advection dominates, concentration  
profiles observed upwind and downwind of an area source can be used in a simple box model to infer the surface flux (Hajny  
et al., 2019; O’Shea et al., 2014; Tomlin et al., 2023; Wratt et al., 2001). In a one-dimensional ABL without horizontal  
advection, the problem is simplified to the surface flux being balanced by the entrainment flux and the time rate of change of  
50 the concentration in the ABL air column (Laubach and Fritsch, 2002; Raupach et al., 1992). This column budget method, also  
called the slab approximation (Lee, 2023), requires that the entrainment flux be calculated as the product of the entrainment  
velocity and the inversion jump of concentration. While the entrainment velocity can be derived from the ABL growth rate or  
a parameterization equation (Vilà-Guerau de Arellano et al., 2004; Trousdell et al., 2016), the inversion jump must be measured.  
(The inversion jump refers to the difference in concentration across the capping inversion at the top of the ABL.) The inversion  
55 jump of CO<sub>2</sub> has been measured in many aircraft-based studies (Barker et al. 2021; Filges et al., 2015; Herrera et al., 2021;  
Laubach and Fritsch, 2002; Lloyd et al., 2001; Narbaud et al., 2023; O’Shea et al., 2014; Saito et al, 2009; Sarrat et al., 2007;  
Shashkov et al., 2007; Shibata et al., 2018; Xueref-Remy et al., 2011). Fewer studies have reported the CH<sub>4</sub> profile with large  
enough vertical span to include the CH<sub>4</sub> inversion jump (Barker et al. 2021; Filges et al., 2015; Hartery et al., 2018; Herrera et  
al., 2021; Narbaud et al., 2023; O’Shea et al., 2014). These CO<sub>2</sub> or CH<sub>4</sub> inversion jump observations were made over forests  
60 (Lloyd et al., 2001, Ramonet et al., 2002, Shashkov et al., 2007), grassland (Vilà-Guerau de Arellano et al., 2004), mixed land  
(cropland and forest; Laubach and Fritsch, 2002; Saito et al., 2009; Sarrat et al., 2007; Shibata et al., 2018), wetlands and  
tundra (Barker et al., 2021; Narbaud et al., 2023; O’Shea et al., 2014; Hartery et al., 2018), and a landscape dominated by  
animal facilities (Herrera et al., 2021). No such data exists yet for urban land.

65 Simultaneous measurement of multiple gases in the ABL can provide a constraint on emission intensity, emission source type  
and source region. Because some gases do not undergo significant chemical reactions over short timescales, the concentration  
ratio is widely used for source identification, for example, to distinguish between anthropogenic and natural sources or to  
indicate the intensity of biomass burning. Examples include C<sub>2</sub>H<sub>6</sub> versus CH<sub>4</sub> (Joo et al., 2024), CH<sub>4</sub> versus CO<sub>2</sub> (Kenea et al.,

2023; Sreenivas et al., 2016) and CO<sub>2</sub> versus CO (Shan et al., 2022). Additionally, it serves as a tool to verify the accuracy of  
70 emission inventories (Hajny et al., 2019; Liu et al., 2018; Shen et al., 2014). The ratio may vary with altitude due to the  
influence of different source and sink processes. In the ABL, the concentrations are primarily affected by local emissions (Park  
et al., 2022). In the free atmosphere, CO<sub>2</sub> and CH<sub>4</sub> concentration variations are influenced by transported air masses (Sreenivas  
et al., 2019). Here, the gas concentration ratio reflects the degree of mixing of the background air with CO<sub>2</sub> and CH<sub>4</sub> emitted  
regionally. When combined with back-trajectory analysis, the ratio can help infer the composition of upwind emission sources  
75 (Shan et al., 2022; Tiemoko et al., 2021). Although some studies have explored the concentration ratio at different altitudes  
downwind of a city and have used it to infer emission origins (Li et al., 2022; Shan et al., 2022), we are not aware of published  
research on the CH<sub>4</sub>:CO<sub>2</sub> ratio in the ABL air column directly above urban land.

Measuring the vertical profiles of CO<sub>2</sub> and CH<sub>4</sub> concentrations in the ABL is challenging due to cost and logistical constraints.  
80 Available measurement platforms include aircraft, tetheredsonde, unmanned aerial vehicle (UAV), and tall tower, each having  
its strengths and weaknesses. Tall towers (Berhanu et al., 2016; Satar et al., 2016) and tetheredsondes (Crawford et al., 2016) can  
provide continuous monitoring, but they can only probe the lower portion of the ABL. Sensors on a tetheredsonde are low-cost  
and lightweight. Having low measurement precision, they are unable to detect small concentration variations in the ABL.  
Recent years have seen increasing use of UAVs (Andersen et al., 2018; Berhanu et al., 2016; Satar et al., 2016; Watai et al.,  
85 2006), but UAV operation also has payload limitation, in addition to aviation restriction on flight height (e.g., no higher than  
120 m above the ground in the USA). Aircraft is the only viable option if gaseous measurements are to extend from the surface  
to the ABL capping inversion. Because gas analyzers on board of an airplane typically have much better precision and faster  
time response than those carried by a tetheredsonde or an UAV, aircraft observation can resolve detailed vertical structures,  
including the concentration jumps across the capping inversion whose thickness is on the order of 50 m. Because of high  
90 operational cost, aircraft observations are carried out in campaign mode with observational time typically less than a few hours.  
Even though aircraft profiles are only snapshot of conditions in the atmosphere, data of this kind makes useful contribution to  
the published literature. In addition to the ABL applications discussed above, they can be used for validation of ground- and  
space-borne sensor retrievals of atmospheric greenhouse gases (Sreenivas et al., 2019; Tanaka et al., 2012) and for evaluation  
of atmospheric transport models (Agustí-Panareda et al., 2023; Friedlingstein et al., 2022; Galkowski et al., 2021; Stephens et  
95 al., 2007; Tomlin et al., 2023; Vogel et al., 2023).

Regarding CO<sub>2</sub> and CH<sub>4</sub> in the urban ABL, Li et al. (2014) collected 58 profiles of CO<sub>2</sub> concentration up to a height of 1400  
m in Xiamen City, China with a portable gas analyzer (measurement uncertainty 4 ppm) attached to a tetheredsonde. These  
profiles showed a clear diurnal pattern, although no inversion jump or a well-mixed layer was evident in the data. Another  
100 tetheredsonde campaign was carried out by Crawford et al. (2016) in Vancouver, Canada over a 24-h period using the same type  
of analyzer as in Li et al. (2014), with a profile height of 400 m. Several authors have reported the CO<sub>2</sub> measurement made  
with commercial airliners equipped with a CO<sub>2</sub> analyzer during their ascent and descent in several large cities in the

CONTRAIL program (Umezawa et al., 2016; Uemzawa et al., 2020). These profiles provide information on the advection of urban emission plumes, but they are less useful for ABL studies because of the lack of data below a height of about 800 m. In  
105 our own examination of the CONTRAIL data (Machida et al., 2018), we could not detect the ABL height or the inversion jump (due to a slow instrument response and the rapid vertical ascent or descent of the aircraft); these two features are critical for accurately estimating emissions using the ABL budget method.

The goal of this study is to characterize the vertical distributions of CO<sub>2</sub> and CH<sub>4</sub> concentrations over four urban areas in  
110 Eastern China. They are, in order from north to south, Beijing, Hengshui, Shangqiu and Nanjing. These profile measurements were made with an analyzer on board of a research airplane that flew a round trip between Beijing and Nanjing. Detailed analysis was made of the observations in Nanjing and Beijing, which were obtained during the plane's landing and take-off and spanned the whole ABL and the lower troposphere. Specifically, we aim (1) to examine the time evolution of the profiles between landing and take-off, (2) to quantify the CO<sub>2</sub> and CH<sub>4</sub> inversion jumps (differences in concentrations across the  
115 capping inversion at the top of the ABL), and (3) to compare the CH<sub>4</sub>:CO<sub>2</sub> emission ratio obtained with the concentration data with the ratio obtained with inventory data.

## **2 Materials and Methods**

### **2.1 Airborne observation**

The airborne observation was conducted in Eastern China on 14 May, 2023 (Figs. 1–3). The flight traversed Beijing, a  
120 province-level municipality, and five provinces (Hebei, Henan, Shandong, Anhui and Jiangsu). Profile measurements were made over Beijing, Hengshui, Shangqiu and Nanjing. Beijing, the capital of China, is located in the North China Plain. It has a permanent population of 21 million and covers an area of 16,000 km<sup>2</sup>. The city is bordered by mountains on the west, north, and northeast sides, while the southeast is characterized by flat plains. The major GHG emission sources include industrial activities, transportation, and household energy consumption. Hengshui is situated in the southeastern part of Hebei Province,  
125 with a permanent population of 4.2 millions and a total area of 8,800 km<sup>2</sup>. The city comprises agricultural land and aquatic landscapes such as Hengshui Lake. GHG emissions primarily originate from industrial manufacturing, while agricultural activities also contribute CH<sub>4</sub> to a certain extent. Shangqiu, located in eastern Henan Province, has a permanent population of 7.7 million and spans an area of 11,000 km<sup>2</sup>. Its terrain is predominantly flat. As a major grain production area and a transportation hub in China, its major emission sources include industrial production and coal mining. Nanjing, the capital of  
130 Jiangsu Province, is located in the lower reaches of Yangtze River. It has a permanent population of 9.5 million and an area of 6,600 km<sup>2</sup>. The urban landscape is a mix of natural and built environments. Industrial production and transportation are the primary sources of emissions in the city.

The aircraft took off from Beijing at 09:44 Beijing time (about 4 h after sunrise), reached an altitude of 2470 m at 09:49 and then flew southward. At 10:57, it started to descend in a spiral pattern from 2410 m to 820 m over Henghui, and then started to ascend at 11:05, reaching an altitude of 6160 m at 11:51 and resuming the southward flight. At 12:38, it spiralled down from 6170 m to 850 m over Shangqiu. After completing this descent at 13:08, it ascended to an altitude of 5250 m at 13:20 and continued its southward flight. It landed in Nanjing at 14:44. The aircraft took off from Nanjing at 18:31, reached an altitude of 5500m at 18:54 and continued the northward travel. It started to descend near Beijing from an altitude of 2200 m at 21:15, and landed in Beijing at 22:17. A total of 8 vertical profiles of CO<sub>2</sub> and CH<sub>4</sub> concentrations were obtained. These are denoted as BJ↑, BJ↓, HS↑, HS↓, SQ↑, SQ↓, NJ↑ and NJ↓, with the upward arrow indicating ascent and the downward arrow indicating descent.

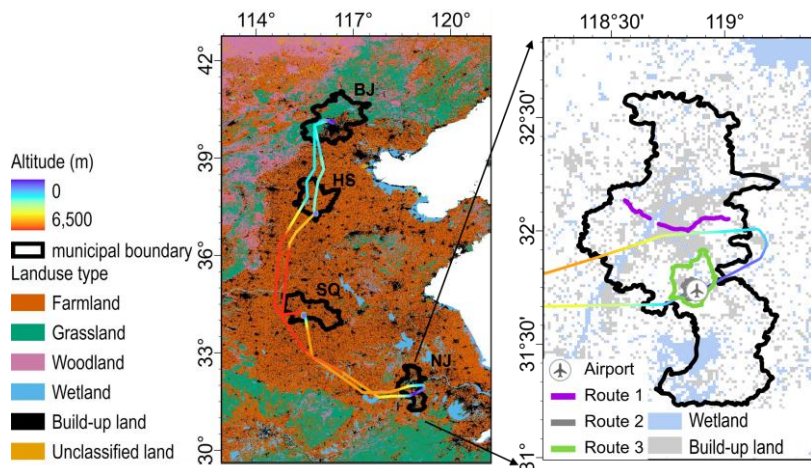


**Figure 1: Left: Locations of the four cities for the vertical profile observations and flight routes; Right: takeoff and landing routes and vehicle-mounted observation routes in Nanjing. The basemap on the left shows wetland and build-up land according to Gong et al. (2019).**

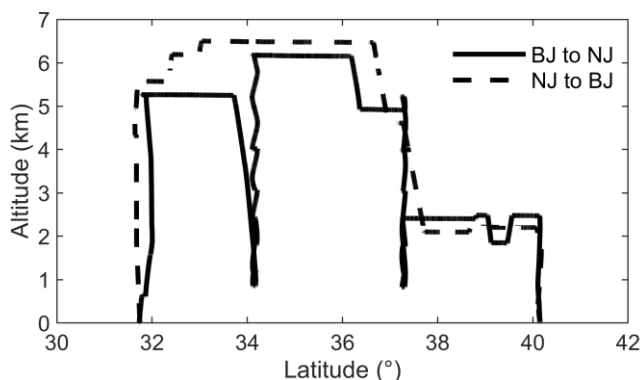


**Figure 2: Flight altitude as a function of latitude. BJ: Beijing; NJ: Nanjing**



150 **Figure 3: Photograph of the airplane (left) and the sampling inlet on the airplane (right)**

A portable CO<sub>2</sub>/CH<sub>4</sub>/H<sub>2</sub>O analyzer based on the off-axis integrated cavity output spectroscopy (model GLA-132-GGA, Los Gatos Research, Mountain View, CA, USA) was used for the airborne observation. It operated in dual modes, one for low pressure and the other for normal atmospheric pressure. The sampling frequency was 1 Hz. Its measurement accuracy was  
155 CH<sub>4</sub> < 2 ppb, CO<sub>2</sub> < 0.3 ppm, H<sub>2</sub>O < 100 ppm. The analyzer was calibrated before the flight. Calibration of water vapor mixing ratio was performed with a dewpoint generator (LI-610, LI-COR Inc., Lincoln, Nebraska, USA) at dewpoints of 1, 5, 10, 15, and 20 °C. Calibration of CO<sub>2</sub> and CH<sub>4</sub> was made with two working standard gases with CO<sub>2</sub> concentrations of 400 ppm and 600 ppm and CH<sub>4</sub> concentrations of 2000 ppb and 3000 ppb. All working standard gases were calibrated with NOAA standard gases before use.

160

The aircraft (King Air model B3587, Beechcraft Aircraft, Fig. 3) was equipped with an air sampling system, including a gas inlet, an aerosol inlet, an external pump and an exhaust. Air was drawn via a sampling tube (Teflon, outer diameter 1/4 inch, length 5.5 m) from the inlet on the top of the aircraft. The inlet was fit with a filter to remove dust particles. The lag time was 1 s. A cold trap was placed upstream of the analyzer to remove most of the moisture in the air sample. The concentration of  
165 the residual moisture was measured by the analyzer; this measurement was used to convert the CO<sub>2</sub> and CH<sub>4</sub> concentrations to molar dry mixing ratios.

In parallel to the gas measurement, an Aircraft Integrated Meteorological Measurement System (AIMMS-20, Aventech Inc., Barrie, Ontario, Canada) was used to measure meteorological variables, including air temperature, humidity and pressure. The  
170 potential temperature and specific humidity were calculated from the observed temperature, humidity and pressure.

## 2.2 Mobile ground-based observation in Nanjing

Ground-based atmospheric CO<sub>2</sub> and CH<sub>4</sub> concentrations were observed along three routes in Nanjing around the time when the aircraft landed (Fig. 1; Fig. S1), using three analyzers (model 915-0011, Los Gatos Research, Mountain View, CA, USA) carried by passenger cars. These analyzers were calibrated before the experiment using the same procedure described above.

175 The air inlet of the analyzer was positioned above the roof of the car, at a height of about 2.5 m above the ground (Hu et al., 2018). Air temperature and air humidity were measured with a Smart-T sensor (Cao et al., 2020) also installed on the top of the car. Route 1 was a 50 km long transect at a distance of about 30 km north of the airport. Measurement started from the west end at 13:00 and reached the eastern end at 15:05. The other two routes formed a large and a small loop around the airport, in a near circular pattern with a radius of 8 and 4 km. Measurement on these routes started at 13:00. The large loop (Route 3)

180 was repeated twice, with the measurement ended at 14:23. The small loop (Route 2) was repeated four times, with the measurement ended at 14:56. Observations made on Routes 2 and 3 were used to compute the mean surface values for comparison with the airborne observation.

## 2.3 Inventory data

The CH<sub>4</sub>:CO<sub>2</sub> emission ratio obtained from airborne observation was compared with the ratio based on the Edgar emission inventory database version 8.0 ([https://edgar.jrc.ec.europa.eu/dataset\\_ghg2024](https://edgar.jrc.ec.europa.eu/dataset_ghg2024)). This is a global inventory product with a spatial resolution of 0.1° × 0.1°. This study uses the inventory data in 2023. First, we calculated the total emission for each city and the corresponding total area within the city administrative boundary. The emission flux (mg m<sup>-2</sup> s<sup>-1</sup>) was then calculated as the ratio of the total emission to the total area.

## 3. Results

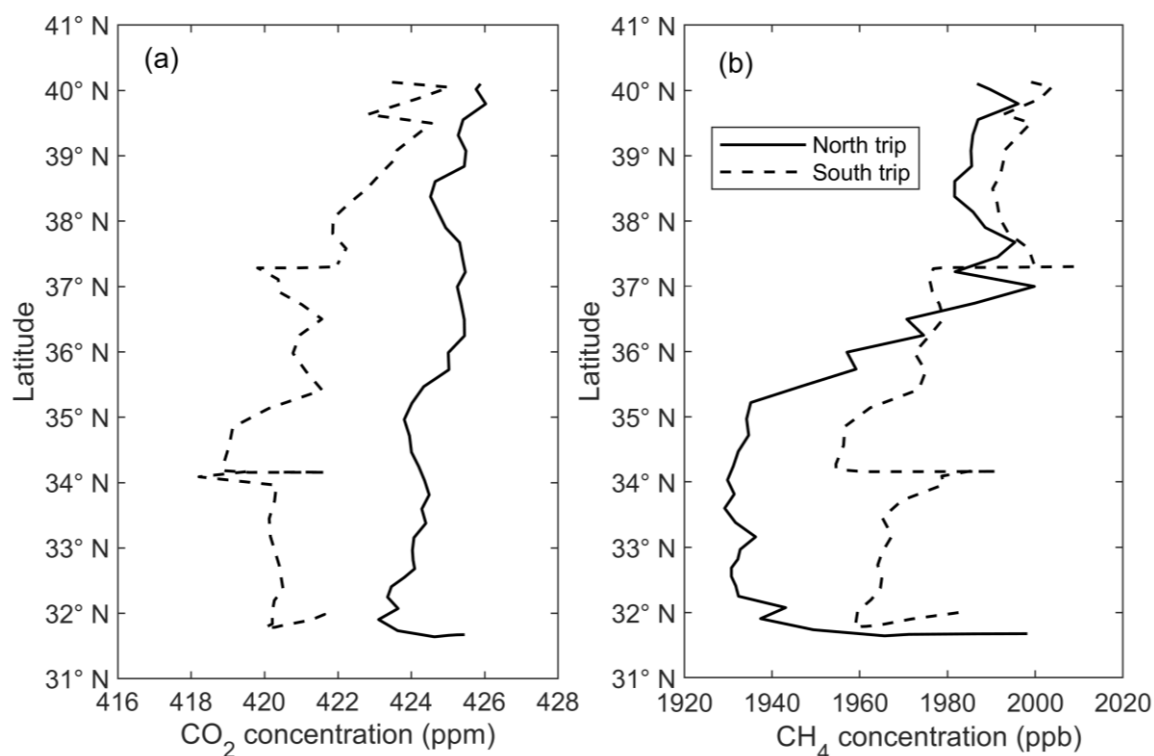
### 190 3.1 Background conditions

According to the surface weather map for 14 May, 2023 (Fig. S2), eastern China was under the influence of a high-pressure system in the south (centered at 28°N and 123°E) and a low-pressure system in the north (centered at 35°N and 118°E). The four components of the surface radiation balance indicate that sky conditions at takeoff and landing were partly cloudy in Beijing and clear in Nanjing (Fig. S3). The surface net radiation at noon was 660.1 W m<sup>-2</sup> in Beijing and 655.6 W m<sup>-2</sup> in

195 Nanjing. On the day of airborne campaign, air pollution levels were moderate in Eastern China, with the surface PM<sub>2.5</sub> concentration ranging from 15 to 46 μg m<sup>-3</sup> (Beijing), 14 to 46 μg m<sup>-3</sup> (Henghsui), 26 to 42 μg m<sup>-3</sup> (Shangqiu), and 23 to 47 μg m<sup>-3</sup> (Nanjing). In Beijing, the surface wind speed was 1.7 m s<sup>-1</sup> (from the northeast) at takeoff and 1.9 m s<sup>-1</sup> (from the northeast) at landing. In Nanjing, the wind speed was 0.5 m s<sup>-1</sup> (from the southwest) at takeoff and 2.3 m s<sup>-1</sup> (from the southwest) at landing.

200

Figure 4 shows the concentrations in the free atmosphere (above 2 km in altitude) as a function of latitude. The overall CO<sub>2</sub> concentration in the south trip (from Beijing to Nanjing) was lower than that in the north trip. The trip mean was  $421.0 \pm 1.5$  ppm for the south trip and  $424.6 \pm 0.9$  ppm for the north trip (from Nanjing to Beijing). These values were 3.3 to 5.3 ppm lower than the concentrations recorded at the WMO surface background sites CPA (Cholpon-Ata, Kyrgyzstan, 42.6369°N, 77.0675°E) and GSN (Gosan, Republic of Korea, 33.29382°N, 126.16283°E) on 14 May, 2023 (Fig. S4). These background observations showed higher CO<sub>2</sub> values in the late afternoon and the evening than in the midday, so the difference between the north and the south trip in the free atmosphere appears to partly reflect the CO<sub>2</sub> diurnal trend in this region. For CH<sub>4</sub>, the concentration shows a latitude dependence, with higher values in more northern latitudes. The CH<sub>4</sub> concentration was similar between the two trips in areas north of 36.5°N. In areas south of 36.5°N, the CH<sub>4</sub> concentration in the south trip was about 30 ppb higher than that in the north trip. The flight height was similar between the two trips in areas north of 36.5°N, but in areas south of this latitude, the flight height was about 1 km lower in the south trip than in the north trip (Fig. 2), implying a vertical CH<sub>4</sub> gradient of  $-30$  ppb km<sup>-1</sup> in the upper troposphere in Eastern China, although some of the difference may have been caused by temporal variations. The trip mean was  $1976 \pm 15$  ppb for the south trip and  $1960 \pm 26$  ppb for the north trip, which were slightly lower than the background concentrations at CPA and GSN (Fig. S4).



215

Figure 4: CO<sub>2</sub> and CH<sub>4</sub> concentrations as a function of latitude. Data are 5 min averages.

### 3.2 Vertical profiles

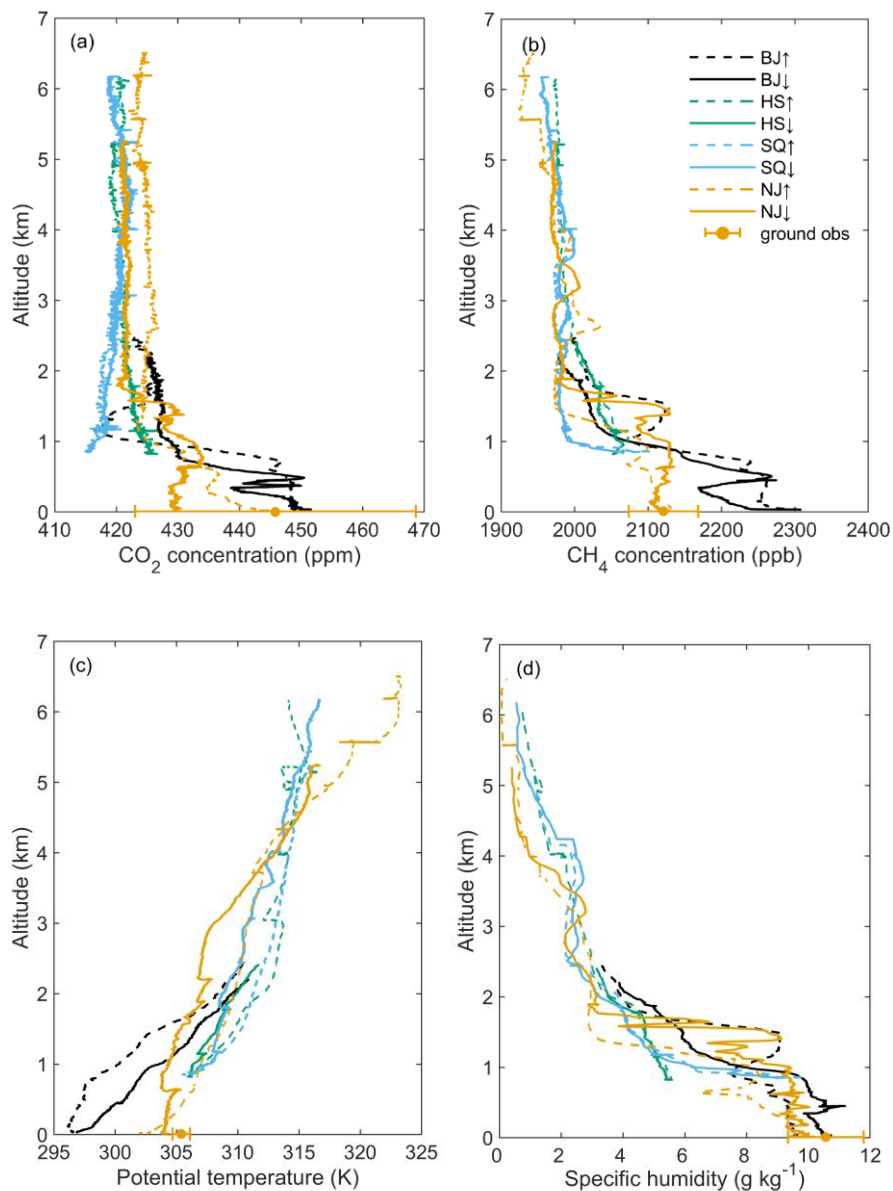
Figure 5 shows the vertical profiles of CO<sub>2</sub>, CH<sub>4</sub>, potential temperature, and specific humidity over the four cities. For Beijing and Nanjing, the profiles extended from the free atmosphere down to the surface, while those over Hengshui and Shangqiu extended down to approximately 850 m above the ground. Two complete observations were made over Beijing. The ascending profiles of CO<sub>2</sub> and CH<sub>4</sub>, observed at about 09:45, indicate the depth of the ABL to be about 800 m. The mean concentrations in the ABL were  $447.5 \pm 1.6$  ppm and  $2251 \pm 20$  ppb for CO<sub>2</sub> and CH<sub>4</sub>, respectively. The potential temperature was not well mixed; instead, an inversion layer, at a strength of about  $5 \text{ K km}^{-1}$ , extended from the 2-km height down to the surface. The specific humidity was more uniform than the potential temperature, changing from  $9.5 \text{ g kg}^{-1}$  at the surface to about  $8.0 \text{ g kg}^{-1}$  at the top of the ABL. The descending profiles, observed at about 22:12, were still influenced by stable stratification. The ABL at this time was shallower than in the morning, with a depth of approximately 500 m as indicated by the CO<sub>2</sub> profile. The mean concentrations below this height ( $444.9 \pm 3.4$  ppm and  $2220 \pm 34$  ppb for CO<sub>2</sub> and CH<sub>4</sub>, respectively) were lower than the mid-morning values. The surface humidity increased to  $10.8 \text{ g kg}^{-1}$ .

Two complete sets of profiles were also obtained over Nanjing. The descending profiles were observed at approximately 14:35. The CO<sub>2</sub>, CH<sub>4</sub> and specific humidity profiles indicate that the ABL height was about 1500 m. The potential temperature was more uniform than in the Beijing ABL, showing near neutral to slightly stable stratification. The mean ABL concentrations were  $431.0 \pm 1.6$  ppm and  $2120 \pm 11$  ppb for CO<sub>2</sub> and CH<sub>4</sub>, respectively. For comparison, the ground-based concentrations, averaged over Routes 2 and 3 (Fig. S1, the two loops around the airport), were  $445.8 \pm 22.8$  ppm and  $2124 \pm 41$  ppb for CO<sub>2</sub> and CH<sub>4</sub>, respectively. The ground-based temperature and specific humidity were slightly greater (by 0.8 K and  $1.3 \text{ g kg}^{-1}$ ) than the surface values observed at the airport by the airborne instruments. The ascending profiles were observed at about 18:31. By this time a surface inversion layer had developed. Although the surface CH<sub>4</sub> at the airport did not change much from that at landing, the surface CO<sub>2</sub> increased to 444.6 ppm at takeoff from 429.6 ppm at landing.

The ground-based CO<sub>2</sub> concentration in Nanjing was 14.8 ppm higher than the average concentration in the ABL at landing, and the CH<sub>4</sub> concentration was 4 ppb higher. These differences might be indicative of strong concentration gradients near the ground. The vehicle-mounted observation was made at 2.5 m above the ground. In comparison, the minimum altitude of the aircraft observation exceeded 20 m. Gao et al. (2018) reported that under low wind conditions, a CO<sub>2</sub> concentration difference up to 40 ppm can develop over a vertical separation of 30 m in the surface air layer in Nanjing. Another reason might be that the CO<sub>2</sub> concentration measured on the routes around the airport (Figure 1) was higher due to stronger traffic influence than at the airport.

The ABL in Beijing in the mid-morning was more enriched in CO<sub>2</sub> and CH<sub>4</sub> than the ABL in Nanjing in the mid-afternoon. The differences in the mean ABL concentrations were 16.5 ppm and 131 ppb for CO<sub>2</sub> and CH<sub>4</sub>, respectively. At night, the CO<sub>2</sub>

250 and CH<sub>4</sub> concentrations in Beijing were also higher than those in Nanjing by 9.4 ppm and 114 ppb, respectively. The ABL specific humidity was similar between the two cities. Both cities were net sources of CO<sub>2</sub> and CH<sub>4</sub>, despite having high fractions of urban greenspaces (50% and 45% for Beijing and Nanjing, respectively).

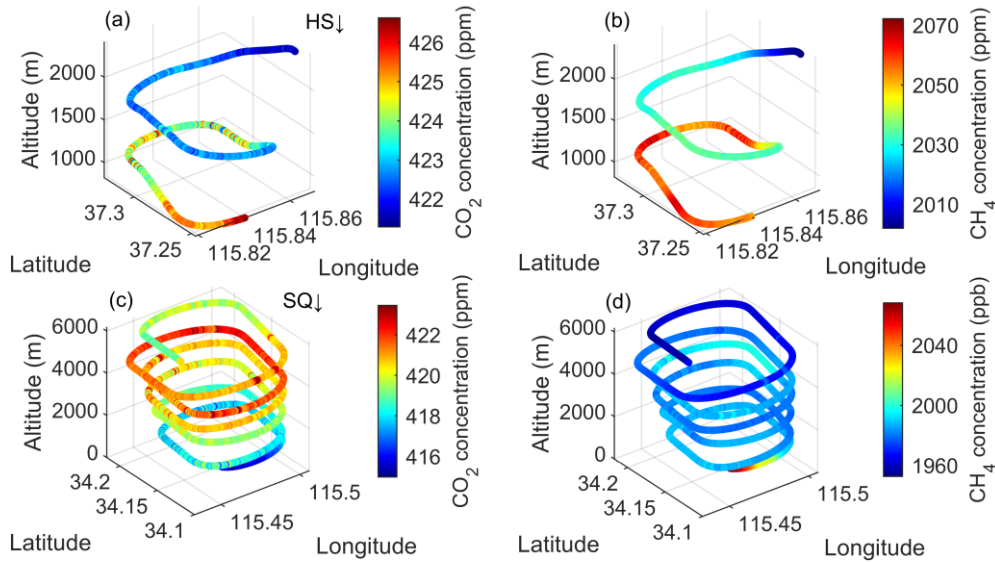


255

**Figure 5: Vertical profiles of atmospheric CO<sub>2</sub> concentration (a), CH<sub>4</sub> concentration (b), potential temperature (c), and specific humidity (d) over the four cities. Red dots: ground-based mean values of the vehicle-mounted measurement around the airport in Nanjing. Data points are 1 Hz observations. BJ: Beijing; NJ: Nanjing; HS: Hengshui; SQ: Shangqiu. The wind profiles were presented in Figure S5.**

260 The profiles over Hengshui and Shangqiu were stopped at 850 m above the ground and did not adequately sample the interior of the ABL. Nevertheless, they indicated that the surface influences on the ABL GHG budgets differed between the two locations. Over these two cities, the ascending and descending CO<sub>2</sub> and CH<sub>4</sub> profiles were nearly identical. The CO<sub>2</sub> concentration showed a decreasing trend with decreasing altitude at Shangqiu, indicating that the surface was a sink of CO<sub>2</sub>, whereas it showed an increasing trend with decreasing altitude at Hengshui, indicating the surface was a source of CO<sub>2</sub>. The  
265 CH<sub>4</sub> concentration showed an increasing trend with decreasing altitude at both locations, reflecting the fact that the surface was a source of CH<sub>4</sub>. The CH<sub>4</sub> concentration experienced a rapid change at Shangqiu, increasing from 1998 ppb at 1000 m to 2102 ppb at 850 m. This step-like change suggests that the capping inversion of occurred between 850 m and 1000 m above the ground at Shangqiu. A sharp change in specific humidity was also observed between 850 m and 1000 m at Shangqiu (Fig 5d). At an altitude of 850 m, the CH<sub>4</sub> concentration reached a high value of 2102 ppm (nearly the same as the mid-afternoon  
270 ABL mean in Nanjing), suggesting that the CH<sub>4</sub> concentration in the ABL at Shangqiu might have been quite high. In other words, the landscape near Shangqiu might be a sink of CO<sub>2</sub> but a strong source of CH<sub>4</sub>, and the landscape near Hengshui might be a source for both CO<sub>2</sub> and CH<sub>4</sub>. Given the lack of ABL sampling, the exact CO<sub>2</sub> and CH<sub>4</sub> concentration in the ABL at Hengshui and Shangqiu remained unknown.

The spiky appearance of the descending profiles at Hengshui and Shangqiu in Fig. 6 was a consequence of the spiral flight  
275 pattern, which mixed horizontal variations with vertical variations (Fig. 6). At Hengshui, the downward spiral started at the altitude of 2413 m and consisted of two loops with the north-south extent of 10 km and the east-west extent of 5.5 km. At Shangqiu, the spiral started at the altitude of 6170 m and consisted of six loops with the north-south extent of 13 km and the east-west extent of 6.5 km. Generally, the CO<sub>2</sub> and CH<sub>4</sub> concentrations exhibited greater variations in the vertical direction than in the horizontal directions. The horizontal variation in CO<sub>2</sub> was about 3 ppm across the spiral loop at the height of about  
280 1.3 km over both cities. In the profile plot in Figure 6a, the data collected in the horizontal flights were collapsed to the same altitudes, giving the appearance of small horizontal spikes (with a spike length of about 3 ppm). The CH<sub>4</sub> concentration had no discernible horizontal variation at this height, and it showed a small horizontal variation of about 10 ppb at an altitude of about 4 km over Shangqiu (Figure 6d).



285 **Figure 6: Profiles of CO<sub>2</sub> and CH<sub>4</sub> over Hengshui (top) and Shangqiu (bottom) measured along downward spiral flight paths.**

### 3.3 Inversion jumps

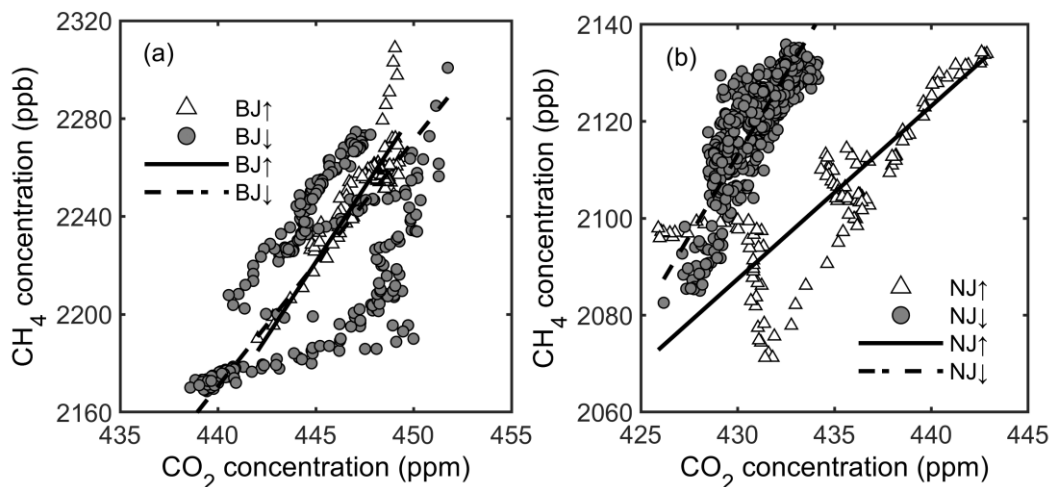
Table 1 summarizes the capping inversion jump values of CO<sub>2</sub>, CH<sub>4</sub>, and specific humidity in Beijing and Nanjing. The actual capping inversion was not visible in the potential temperature profile because of the slow time response of the temperature sensor (The thermistor responds in under a second, but during climb or descent its effective response can stretch to several  
 290 seconds to about a minute). To determine the jump values, we calculated the average concentrations below 800 m for the midday observation and 500 m for the nighttime observation over Beijing, and below 1500 m for the mid-afternoon observation and 1000 m for the early evening observation over Nanjing, to represent the concentrations in ABL. The average concentration  
 in the 1–2 km layer over Beijing and that in the 2–3 km layer over Nanjing was used as the average concentration of the lower free atmosphere. The difference between the average concentration in the ABL and that of the free atmosphere was taken as  
 295 the inversion jump. For CO<sub>2</sub>, the inversion jump value in Beijing was  $-25.2 \pm 0.4$  ppm in the mid-morning and  $-18.0 \pm 0.2$  ppm at night, indicating a larger vertical gradient during the day. In Nanjing, the CO<sub>2</sub> inversion jump value was  $-9.5 \pm 0.1$  ppm in mid-afternoon and  $-10.0 \pm 0.4$  ppm in the early evening, showing an opposite trend to Beijing. For CH<sub>4</sub>, the inversion jump value in Beijing increased slightly in magnitude with time, from  $-171.4 \pm 4.2$  ppb in the mid-morning to  $-202.6 \pm 2.3$  ppb at night. A decreasing magnitude was observed in Nanjing, where the CH<sub>4</sub> inversion jump value changed from  $-140.7 \pm$   
 300  $0.1$  ppb in the mid-afternoon to  $-108.0 \pm 2.1$  ppb in the early evening. For specific humidity, the inversion jump in Nanjing was higher in magnitude than in Beijing.

305 **Table 1: Inversion jumps of specific humidity, CO<sub>2</sub> and CH<sub>4</sub> over Beijing and Nanjing**

Take-off/landing time	Beijing		Nanjing	
	09:44	22:17	14:44	18:31
CO <sub>2</sub> (ppm)	-25.2 ± 0.4	-18.0 ± 0.2	-9.5 ± 0.1	-10.0 ± 0.4
CH <sub>4</sub> (ppb)	-171.4 ± 4.2	-202.6 ± 2.3	-140.7 ± 0.1	-108.0 ± 2.1
Specific humidity (g kg <sup>-1</sup> )	-2.02 ± 0.18	-4.90 ± 0.04	-6.62 ± 0.04	-5.80 ± 0.07

### 3.4 CH<sub>4</sub> and CO<sub>2</sub> correlation

Figure 7 shows the correlation between CO<sub>2</sub> and CH<sub>4</sub> concentrations in the ABL in Beijing and Nanjing. A highly significant correlation was observed between the concentrations of the two gases in both cities ( $p < 0.01$ ). In Beijing, the data collected during the mid-morning take-off (ascending) and during the evening landing (descending) were clustered together. The mid-morning regression slope was 12.22 ppb ppm<sup>-1</sup>, with a correlation coefficient ( $r$ ) of 0.87. At night, the slope decreased to 10.03 ppb ppm<sup>-1</sup>, and  $r$  was 0.65. The Nanjing data showed a clear separation between takeoff and landing, with lower CO<sub>2</sub> and CH<sub>4</sub> concentrations at landing (descending) in the mid-afternoon than at takeoff (ascending) in the early evening. The midafternoon regression slope was 6.71 ppb ppm<sup>-1</sup> with an  $r$  value of 0.83, while the early evening slope was 3.57 ppb ppm<sup>-1</sup> with an  $r$  of 0.78. The regression slopes for Beijing were nearly twice those observed in Nanjing, reflecting a stronger urban CH<sub>4</sub> source in Beijing (section 4.1). The correlation between the two gases were stronger for Nanjing than for Beijing, probably because the ABL was better developed in Nanjing. In comparison, the free-atmospheric ratio over Beijing and Nanjing diverged significantly (Fig. S6).



320 **Figure 7: Correlation between CO<sub>2</sub> and CH<sub>4</sub> concentrations in the ABL (a: Beijing; b: Nanjing). Each data point represents 1 s sampling**

The two gases were highly correlated in the free atmosphere (altitude greater than 2 km; Fig. 8). The correlation was significant for both trips ( $r > 0.73$ ,  $p < 0.001$ ). The data during these two trips form two distinct clusters. The regression slope of the south trip was  $10.01 \text{ ppb ppm}^{-1}$ , which falls between the free tropospheric values observed over Hengshui and Shangqiu (Figure S7).  
325 The regression slope of the north trip was much higher, at  $29.95 \text{ ppb ppm}^{-1}$ .

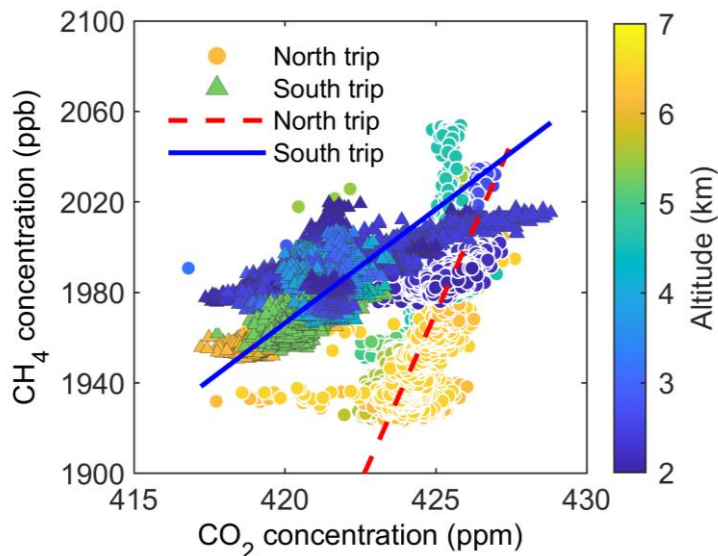


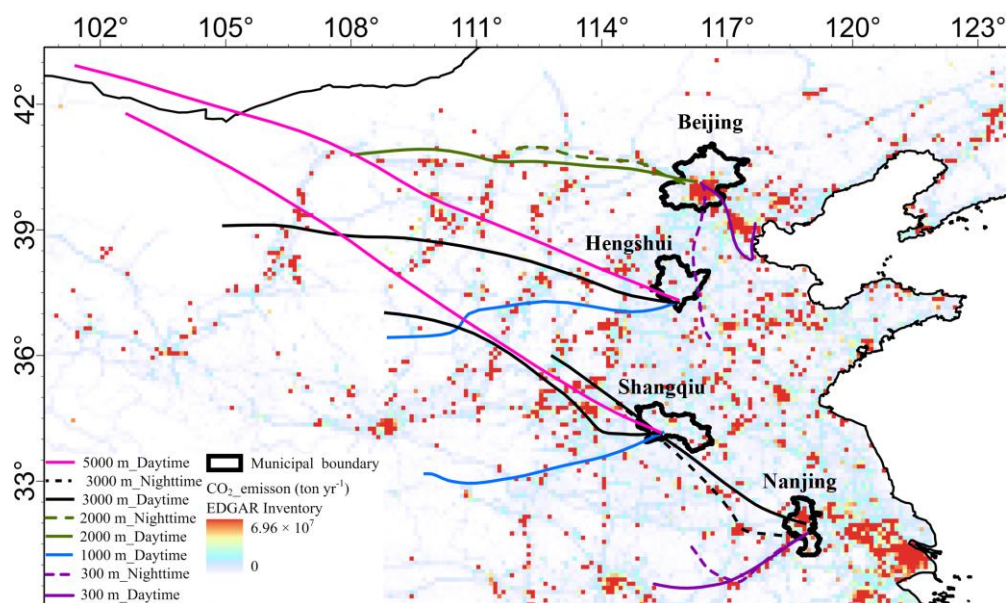
Figure 8: Correlation between CO<sub>2</sub> and CH<sub>4</sub> concentrations above 2 km. Data points are 1 Hz observations.

## 4. Discussion

### 330 4.1 Contrasts among the four cities

We compared the EDGAR emission inventory data with the observed concentration profiles. The CO<sub>2</sub> and CH<sub>4</sub> concentrations in the four cities were inconsistent with the inventory products. The EDGAR CO<sub>2</sub> emission flux of the four cities was, in order from the highest to the lowest, Nanjing ( $0.58 \text{ mg m}^{-2}\text{s}^{-1}$ ), Beijing ( $0.16 \text{ mg m}^{-2}\text{s}^{-1}$ ), Shangqiu ( $0.11 \text{ mg m}^{-2}\text{s}^{-1}$ ) and Hengshui ( $0.058 \text{ mg m}^{-2}\text{s}^{-1}$ ). However, the CO<sub>2</sub> concentration in Beijing was much higher than that in Nanjing, and the concentration at  
335 850 m (the lowest observation altitude) in Hengshui was also higher than that in Shangqiu. For CH<sub>4</sub>, the emission flux order was Nanjing ( $1.35 \text{ } \mu\text{g m}^{-2} \text{ s}^{-1}$ ), Beijing ( $0.67 \text{ } \mu\text{g m}^{-2} \text{ s}^{-1}$ ), Shangqiu ( $0.56 \text{ } \mu\text{g m}^{-2} \text{ s}^{-1}$ ) and Hengshui ( $0.32 \text{ } \mu\text{g m}^{-2} \text{ s}^{-1}$ ). But again, the CH<sub>4</sub> concentration in Beijing was higher than that in Nanjing. These contrasts urge caution against using the concentrations as indication of emission strengths. We note that the profiles in Figure 5 were sampled at different times of the day. Some of the differences may have been caused by changing atmospheric conditions. The general inter-city patterns were unaffected  
340 because the temporal differences in the concentrations sampled at takeoff and at landing were smaller than the between-city differences.

Four possible factors might account for the discrepancies between the emission inventory data and the concentrations in Beijing and Nanjing. One possible reason was spatial heterogeneity of the surface emission sources. In Nanjing, the CO<sub>2</sub> and CH<sub>4</sub> emission inventories included four and three grids with abnormally high emission values, respectively. These grids, located at 30 to 60 km to the north of the airport, were missed by the air trajectory arriving in the ABL in Nanjing (Fig. 9 below & Fig. S8). After removing these grids, the CO<sub>2</sub> and CH<sub>4</sub> emission fluxes in Nanjing decreased to 0.22 mg m<sup>-2</sup> s<sup>-1</sup> and 1.13 μg m<sup>-2</sup> s<sup>-1</sup>, respectively. The CO<sub>2</sub> emission flux was only about 38% of the original value, and the CH<sub>4</sub> emission flux also decreased accordingly. The second possible reason was the difference in mixing efficiency in the ABL. The ABL height in Beijing was approximately half that in Nanjing, which would result in higher average concentrations in the Beijing ABL. The third reason was the difference in vegetation photosynthetic efficiency. Although the NDVI in Beijing (0.54) was similar to that in Nanjing (0.53) during the experimental period, the growing season was still early in Beijing and the plant photosynthetic uptake of CO<sub>2</sub> was likely lower than that in Nanjing. The fourth possible reason was advection. As an air mass moves, it continuously accumulates emissions from the surface along its path, leading to higher concentrations in downwind areas. More CO<sub>2</sub> might have been accumulated near the surface in Beijing than in Nanjing. Overall, these four factors might explain the lack of agreement between the emission inventory and the observed concentrations.



360 **Figure 9: Backward trajectories of air mass at different end heights. Background map shows the EDGAR CO<sub>2</sub> emission inventory with the color scale indicating annual emission amount per 0.1° by 0.1° grid. Trajectory length is 24 h.**

## 4.2 Influence of airmass trajectories

In the idealized one-dimensional urban boundary layer, the CO<sub>2</sub> and CH<sub>4</sub> emitted by sources in the city are trapped in a dome above the city. Their vertical profiles and time changes are shaped by the surface emission, vertical mixing and exchanges with the free atmosphere. Horizontal advection does not play a role. In this study, the ABL deviates from this idealization because the vertical concentration profiles were also influenced by airmass advection. Fig. 9 illustrates the sources of air mass at different altitudes in each city. In Fig. 9, the basemap shows the EDGAR CO<sub>2</sub> emission flux. The same trajectories are also plotted against the EDGAR CH<sub>4</sub> emission map (Fig. S8). The concentrations within the ABL in Beijing and Nanjing were influenced by short-range transport and local emissions. In Beijing, the daytime air mass trajectory passed through high-emission areas located to the southwest of the city, whereas at night, few high-emission areas were present along the trajectory. This pattern was consistent with the higher CO<sub>2</sub> and CH<sub>4</sub> concentrations at the height of around 300 m in the daytime than at night (Fig. 5 a & b).

In Nanjing, the backward trajectories in the ABL at landing and at take-off were similar. The observed higher CO<sub>2</sub> concentration at the evening take-off (Fig. 5a) might have been caused by accumulation of locally-emitted CO<sub>2</sub> in the ABL. Interestingly, the CH<sub>4</sub> concentration near the surface experienced little change between these two times. It appears that at the evening takeoff, the CO<sub>2</sub> concentration was influenced heavily by vehicle emissions near the airport, whereas the CH<sub>4</sub> concentration was influenced by more distance sources such as landfills. This is a reason for why the ABL data for Nanjing in Fig. 7 exhibits two distinct clusters for the takeoff and landing.

In the free atmosphere, the GHG concentrations were mainly controlled by long-range air mass transport. The CO<sub>2</sub> concentration above 3 km in Nanjing was about 3 ppm higher at takeoff than at landing (Fig. 5a). The backward trajectories indicate that during landing, the air mass passed over regions with relatively low CO<sub>2</sub> emissions (Fig. 9). At takeoff a few hours later, the air mass passed through Huainan, a city with intensive energy and chemical industries, and Hefei, the provincial capital of Anhui Province. The variation in air mass trajectories also resulted in changes in the ratios above Hengshui and Shangqiu (Fig. S7).

Previous studies have similarly concluded that advection of airmass exert a large influence on GHG concentrations. Airmass trajectory patterns are responsible for synoptic-scale variability of CO<sub>2</sub> and CH<sub>4</sub> concentrations at a regional background site on the west coast of South Korea (Kenea et al., 2023). Liu et al. (2025) presented two AirCore profiles of CO<sub>2</sub> over Hangzhou, a city about 200 km to the southeast of Nanjing, with one influenced by northeasterly flow and the other by southeasterly flow. The second profile shows consistently higher concentration by about 3 ppm than the first profile between the 2 and 25 km altitude, a difference similar to that we observed between take-off and landing in Nanjing (Fig. 5a). In an airborne field campaign over Bhubaneswar, Varanasi and Jodhpur of India, Sreenivas et al. (2019) observed that high CO<sub>2</sub> concentration

below the 1 km altitude is associated with northwesterly flow. Umezawa et al. (2016) reported that the CO<sub>2</sub> concentration  
395 observed by an CONTRAIL aircraft over Delhi, India shows decreasing trends towards the ground on some days and increasing  
trends on other days; these fluctuations were associated with synoptic weather conditions that presumably altered air mass  
trajectories and therefore the relative roles of CO<sub>2</sub> uptake by the cropland near the city and CO<sub>2</sub> emission in the city. In an  
expanded analysis of the CONTRAIL data, Umezawa et al. (2022) showed that the CO<sub>2</sub> concentration at 1.0-1.5 km altitude  
is enhanced than the background by 1 to 6 ppm if the air mass trajectory passes a major city. They also reported that this local  
400 urban influence on the CO<sub>2</sub> concentration between the 4.0 and 4.5 altitude is weaker.

### 4.3 CO<sub>2</sub>: CH<sub>4</sub> ratio

The CH<sub>4</sub>:CO<sub>2</sub> ratio in the ABL can serve as an independent check on the accuracy of emission inventories. Table 2 compares  
the ratios determined with the concentration observations and those with inventory data. According to the EDGAR inventory  
data, the CH<sub>4</sub>:CO<sub>2</sub> emissions ratio was 11.72 ppb ppm<sup>-1</sup> for Beijing and 6.48 ppb ppm<sup>-1</sup> for Nanjing. To minimize the influence  
405 of photosynthetic CO<sub>2</sub> uptake, we compared these with the aircraft-observed ratios at night. Results showed that the inventory  
ratio was within the measurement uncertainty in Beijing and was higher by about 80% in Nanjing. Several factors may have  
contributed to the mismatch in Nanjing. First, vehicle and waste management are the two major CH<sub>4</sub> emission sources in  
Nanjing. In the last decade, vehicle fleets in Chinese cities have experienced two shifts in fuel use, first from gasoline to natural  
gas and then from gasoline and natural gas to electric (Hao et al., 2016; China's Energy Transition, 2024). These transitions  
410 were not accounted for by the EDGAR inventory. Second, using an inversion modeling with CH<sub>4</sub> concentration data, Hu et al.  
(2023) estimated that EDGAR CH<sub>4</sub> emission in Hangzhou is biased high by about 50% primarily due to a high bias for the  
waste management sector. It is possible that this source category was also biased high for Nanjing because Nanjing and  
Hangzhou, both located in the YRD, use similar methods to manage waste. Third, residents in Nanjing use natural gas for  
space heating. The inventory data are annual mean values that include contributions from space heating, whereas the aircraft  
415 observation was made in late spring when space heating was no longer needed. Finally, this study used the nighttime  
concentration ratio for comparison, an approach that can reduce, but not eliminate, the influence of the biosphere on CO<sub>2</sub>.  
Addition of a typical respiration CO<sub>2</sub> flux of 0.1 mg CO<sub>2</sub> m<sup>-2</sup> s<sup>-1</sup> to the EDGAR CO<sub>2</sub> emission would reduce the inventory  
emissions ratio in Nanjing to 5.46 ppb ppm<sup>-1</sup>. The relative roles of these factors cannot be inferred from one profile sampling,  
and a firm conclusion will require more observational data, a better estimate of biospheric respiration, and allocation of the  
420 annual inventory total to seasons and daytime and nighttime.

425

**Table 2: CH<sub>4</sub>:CO<sub>2</sub> emissions ratios obtained with the ABL concentration data, the inversion jump values and the EDGAR inventory data**

	Beijing (ppb ppm <sup>-1</sup> )		Nanjing (ppb ppm <sup>-1</sup> )	
Take-off/landing time	09:45	22:12	14:35	18:33
Concentration	12.22 ± 1.21	10.03 ± 0.90	6.71 ± 0.32	3.57 ± 0.42
Entrainment	6.79 ± 0.28	11.28 ± 0.25	14.84 ± 0.15	10.80 ± 0.64
Inventory	11.72		6.48	

430 Table 2 also presents the ratio of the CH<sub>4</sub> to the CO<sub>2</sub> entrainment flux at the ABL top. Since the entrainment velocity is the  
435 same for both gases, the entrainment flux ratio is equivalent to the ratio of the inversion jump values shown in Table 1. This  
flux ratio was close to the ratio derived from the ABL concentration data in Beijing at night, but it was lower than the ABL  
ratio during the day. In Nanjing where the ABL was well developed, the entrainment flux ratio was much greater than the ABL  
ratio at both times. These results suggest that the one-dimensional slab approximation (Chapter 11; Lee, 2023) may be too  
440 simplistic for the urban ABL. In this approximation, there is no advective influence. Using large-eddy simulations, Huang et  
al. (2011) showed that in a fully developed one-dimensional ABL under steady state, the entrainment CO<sub>2</sub> flux is approximately  
equal to the surface CO<sub>2</sub> flux. This equality should also hold for CH<sub>4</sub> because like CO<sub>2</sub>, CH<sub>4</sub> is conserved trace gas and without  
a source or sink above the ABL, implying equality of the CH<sub>4</sub>:CO<sub>2</sub> flux ratio at the surface and at the ABL top. However, in  
an evolving ABL, the surface and the entrainment CO<sub>2</sub> flux can be quite different (Vilà-Guerau de Arellano et al., 2004).  
Furthermore, as air moves from the rural background into the urban domain, its CH<sub>4</sub> and CO<sub>2</sub> concentrations will increase with  
445 downwind distance (Gao et al., 2018). This advection contribution to the urban ABL GHG budgets was likely important. An  
analogous situation exists in the European Arctic wetlands, where the ABL air becomes gradually enriched in CH<sub>4</sub> and depleted  
in CO<sub>2</sub> as it moves across the region (O'Shea et al., 2014), but unlike the urban land in Nanjing where the surface was a net  
source of both CO<sub>2</sub> and CH<sub>4</sub>, these wetlands are a source of CH<sub>4</sub> and a sink of CO<sub>2</sub>.

445 In the free atmosphere, the ratio obtained during the north trip was about three times that during the south trip (Fig. 8). The  
observed difference is likely caused by the difference in flight altitude. In latitudes between 33.0°N and 36.5°N, the airplane flew  
at a cruising altitude of 6.5 km during the north trip, which was 0.5 to 1.3 km greater than during the south trip. At this altitude,  
the CH<sub>4</sub> concentration was lower than at lower altitudes (Fig. 4b). If we exclude the data obtained above 5.5 km, the data collected  
during the two trips would collapse to a similar clustering pattern (Fig. 8).

#### 450 4.4 Inversion jumps

The CO<sub>2</sub> and CH<sub>4</sub> inversion jumps reveal information about the role of entrainment at the ABL top. The entrainment flux is  
proportional to the jump value. If the jump value is positive ((higher concentration in the free atmosphere than in the ABL),

entrainment will enrich the gas in the ABL. If the jump value is negative (lower concentration in the free atmosphere), entrainment will deplete the gas in the ABL.

455

Our study appears to be the first to report the CO<sub>2</sub> and CH<sub>4</sub> inversion jumps in the urban ABL. Unlike previous studies targeting concentrations in urban plumes or in the urban surface layer, this study directly observed the vertical structures of CO<sub>2</sub> and CH<sub>4</sub> above cities. Crawford et al. (2016) and Li et al. (2014) obtained CO<sub>2</sub> profile data in the ABL in Vancouver, Canada and Xiamen, China, respectively, using tether sondes, but their analyzers did not have enough precision and fast enough time response to resolve the sharp CO<sub>2</sub> concentration change across the capping inversion. Our inversion jump values were negative for both daytime and nighttime, indicating the dominant contributions of anthropogenic emissions to the urban ABL CO<sub>2</sub> and CH<sub>4</sub> budgets. The CO<sub>2</sub> inversion jump reported by other authors for vegetated landscapes can be negative (higher CO<sub>2</sub> concentration in the ABL) or positive (higher CO<sub>2</sub> concentration in the free atmosphere), depending on time of the day. For example, Lloyd et al. (2001) reported a CO<sub>2</sub> inversion jump of about +10 ppm above a forest and wetland mosaic in central Siberia in the mid-afternoon. Vilà-Guerau de Arellano et al. (2004) observed a CO<sub>2</sub> inversion jump of -20 ppm above a cropland landscape in the early morning. Several studies have reported the CH<sub>4</sub> profile with large enough vertical span over the full ABL (Barker et al. 2021; Filges et al., 2015; Hartery et al., 2018; Narbaud et al., 2023; O'Shea et al., 2014); Generally, the CH<sub>4</sub> inversion jump in these profiles is too weak and cannot be determined precisely. One exception is Hartery et al. (2018), who showed a profile over the Alaskan permafrost region with a CH<sub>4</sub> inversion jump of about -10 ppb, which is smaller by an order of magnitude than the values given in Table 1.

460  
465  
470

## 5. Summary and future outlook

The airborne experiment yielded CO<sub>2</sub> and CH<sub>4</sub> concentration data in the ABL over four cities (Beijing, Hengshui, Shangqiu, and Nanjing) and in the free atmosphere (2.0 to 6.5 km above the sea level) in Eastern China. Based on the observations, four key results are summarized as follows:

- 475 (1) Complete vertical profiles in Beijing and Nanjing: the concentrations of CO<sub>2</sub> and CH<sub>4</sub> were higher in the ABL than those in the free atmosphere. In Beijing, the CO<sub>2</sub> inversion jump value was  $-25.2 \pm 0.4$  ppm at takeoff in the mid-morning (09:45 Beijing time) and  $-18.0 \pm 0.2$  ppm at landing in the evening (22:12). In Nanjing, the jump value was  $-9.5 \pm 0.1$  ppm at landing in the afternoon (14:35) and  $-10.0 \pm 0.4$  ppm at takeoff in the early evening (18:33). For CH<sub>4</sub>, the inversion jump in Beijing were  $-171.4 \pm 4.2$  ppb at takeoff and  $-202.6 \pm 2.3$  ppb at landing, while in Nanjing it was  $-140.7 \pm 0.1$  ppb at landing and  $-108.0 \pm 2.1$  ppb at takeoff.
- 480 (2) Partial vertical profiles in Hengshui and Shangqiu: In its spiral descent, the airplane detected variations of about 3 ppm in CO<sub>2</sub> and 0 to 10 ppb in CH<sub>4</sub> over horizontal distances of 5.5 to 13 km in the free atmosphere above the ABL. Below the height of 3 km, the two concentrations were positively correlated in Hengshui and negatively correlated in Shangqiu, indicating that the landscape in Hengshui was a CO<sub>2</sub> source and that in Shangqiu was a CO<sub>2</sub> sink.

- 485 (3) CH<sub>4</sub>:CO<sub>2</sub> ratio: The CH<sub>4</sub>:CO<sub>2</sub> emissions ratio inferred from the nighttime ABL concentration data was within the measurement uncertainty in Beijing and was higher by about 80% in Nanjing. One possible reason is that the inventory did not account for the recent energy transition from gasoline and natural gas to electric in the transport sector. The emissions ratio measured in the well-developed ABL in Nanjing was only about half of the ratio of the CH<sub>4</sub> to CO<sub>2</sub> entrainment flux at the ABL top, calling into question about the suitability of the one-dimensional slab approximation for the urban ABL.
- 490
- (4) Concentrations in the free atmosphere: The mean CO<sub>2</sub> concentration during the evening flight from Nanjing to Beijing was 3.6 ppm greater than the mean concentration during the daytime flight from Beijing to Nanjing. In terms of CH<sub>4</sub>, the concentration showed latitude and altitude dependence, with higher values in more northern latitudes and at lower altitudes. In latitudes between 32.0°N and 36.5°N, the concentration difference between the south and the north trip implies a vertical
- 495 CH<sub>4</sub> gradient of  $-30 \text{ ppb km}^{-1}$  in the upper troposphere.

In this paper, we focused on the CO<sub>2</sub> and CH<sub>4</sub> characteristics in the urban boundary layer. The dataset accompanying this paper can also be used for validation of satellite retrievals and atmospheric transport models (Liu et al. 2025; Sreenivas et al., 2019). Our results suggest that the simple one-dimensional slab model of the convective ABL may be inadequate for describing GHG

500 budgets in the urban environments. An alternative is the advection-entrainment-diffusion model described by Lee (2023; Chapter 12). This model requires observing variations in both the vertical and the horizontal directions.

Future airborne missions should consider a spiral descent or ascent flight pattern over the target city, but unlike the patterns shown in Fig. 6, it should be extended to the lower portion of the ABL. This measurement strategy would yield information

505 on both the ABL vertical structure and horizontal gradients in the ABL. Instead of sampling multiple cities, repeated profiles over time at the same city would allow better evaluation of the ABL dynamics and entrainment influence. Furthermore, winter season is preferred to reduce the confounding effect of biological fluxes.

### **Data availability**

The dataset described in this paper is available at <https://doi.org/10.7910/DVN/ZPVSUVU>.

### **510 Author contributions**

JW: Data curation, Writing (original draft preparation); HX: Data curation; WX: Funding acquisition, Project administration, Supervision, Writing (review and editing); YP: Data curation; NH: Methodology, Validation; JX: Methodology, Validation; YL: Methodology, Validation; LB: Validation; CC: Validation; ZY: Data curation; TW: Data curation; LJ: Investigation; JW: Investigation; MZ: Methodology, Validation; XL: Supervision; Writing (review and editing).

## 515 **Competing interests**

The authors declare that they have no conflict of interest.

## **Disclaimer**

Publisher's note: Copernicus Publications remains neutral with regard to jurisdictional claims made in the text, published maps, institutional affiliations, or any other geographical representation in this paper. While Copernicus Publications makes every effort to include appropriate place names, the final responsibility lies with the authors. Views expressed in the text are those of the authors and do not necessarily reflect the views of the publisher.

## **Financial support**

This work was supported by the Jing-Jin-Ji Regional Integrated Environmental Improvement-National Science and Technology Major Project of Ministry of Ecology and Environment of China (2025ZD1200903), Key Laboratory of Ecosystem Carbon Source and Sink, China Meteorological Administration (ECSS-CMA202302, ECSS-CMA202404), the National Natural Science Foundation of China (U24A20590), the "333 Project" of Jiangsu Province (BRA2022023), and the Joint Funds of the Zhejiang Provincial Natural Science Foundation of China (LZJMZ23D050002).

## **References**

- Agustí-Panareda, A., Barré, J., Massart, S., Inness, A., Aben, I., Ades, M., Baier, B.C., Balsamo, G., Borsdorff, T., Bousseret, N., Boussetta, S., Buchwitz, M., Cantarello, L., Crevoisier, C., Engelen, R., Eskes, H., Flemming, J., Garrigues, S., Hasekamp, O., Huijnen, V., Jones, L., Kipling, Z., Langerock, B., McNorton, J., Meilhac, N., Noël, S., Parrington, M., Peuch, V.-H., Ramonet, M., Razinger, M., Reuter, M., Ribas, R., Suttie, M., Sweeney, C., Rarniewicz, J., and Wu, L.: Technical note: The CAMS greenhouse gas reanalysis from 2003 to 2020. *Atmos. Chem. Phys.*, 23, 3829–3859. <https://doi.org/10.5194/acp-23-3829-2023>, 2023.
- Andersen, T., Scheeren, B., Peters, W., and Chen, H.: A UAV-based active AirCore system for measurements of greenhouse gases. *Atmos. Meas. Tech.*, 11, 2683–2699. <https://doi.org/10.5194/amt-11-2683-2018>, 2018.
- Barker, P. A., Allen, G., Pitt, J. R., Bauguutte, S. J. B., Pasternak, D., Cliff, S., France, J. L., Fisher, R. E., Lee, J. D., Bower, K. N., and Nisbet, E. G.: Airborne quantification of net methane and carbon dioxide fluxes from European Arctic wetlands in Summer 2019. *Phil. Trans. R. Soc., A*, 380, 20210192. <https://doi.org/10.1098/rsta.2021.0192>, 2021.
- Berhanu, T. A., Satar, E., Schanda, R., Nyfeler, P., Moret, H., Brunner, D., Oney, B., and Leuenberger, M.: Measurements of greenhouse gases at Beromünster tall-tower station in Switzerland. *Atmos. Meas. Tech.*, 9, 2603–2614. <https://doi.org/10.5194/amt-9-2603-2016>, 2016.

- Cao, C., Yang, Y., Lu, Y., Schultze, N., Gu, P., Zhou, Q., Xu, J., and Lee, X.: Performance evaluation of a smart mobile air temperature and humidity sensor for characterizing intracity thermal environment. *J. Atmos. Ocean. Technol.* 37, 1891–1905. 545 <https://doi.org/10.1175/JTECH-D-20-0012.1>, 2020.
- Crawford, B., Christen, A., and McKendry, I.: Diurnal course of carbon dioxide mixing ratios in the urban boundary layer in response to surface emissions. *J Appl. Meteorol. Clim.*, 55, 507–529. <https://doi.org/10.1175/JAMC-D-15-0060.1>, 2016.
- Denmead O. T., Raupach M. R., Dunin F. X., Cleugh H. A., and Leuning R.: Boundary layer budgets for regional estimates of scalar flux. *Global Change Biol.*, 2, 255–264. <https://doi.org/10.1111/j.1365-2486.1996.tb00077.x>, 1996.
- 550 Filges, A., Gerbig, C., Chen, H., Franke, H., Klaus, C., and Jordan, A.: The IAGOS-core greenhouse gas package: A measurement system for continuous airborne observations of CO<sub>2</sub>, CH<sub>4</sub>, H<sub>2</sub>O and CO. *Tellus, Ser. B Chem. Phys. Meteorol.*, 6, 27989. <https://doi.org/10.3402/tellusb.v67.27989>, 2015.
- Friedlingstein, P., Jones, M. W., O'Sullivan, M., Andrew, R. M., Bakker, D. C. E., Hauck, J., Le Quééré, C., Peters, G. P., Peters, W., Pongratz, J., Sitch, S., Canadell, J. G., Ciais, P., Jackson, R. B., Alin, S. R., Anthoni, P., Bates, N. R., Becker, M., Bellouin, 555 N., Bopp, L., Chau, T. T. T., Chevallier, F., Chini, L. P., Cronin, M., Currie, K. I., Decharme, B., Djeutchouang, L., Dou, X., Evans, W., Feely, R. A., Feng, L., Gasser, T., Gilfillan, D., Gkritzalis, T., Grassi, G., Gregor, L., Gruber, N., Gürses, Ö., Harris, I., Houghton, R. A., Hurtt, G. C., Iida, Y., Ilyina, T., Lujikx, I. T., Jain, A. K., Jones, S. D., Kato, E., Kennedy, D., Klein Goldewijk, K., Knauer, J., Korsbakken, J. I., Körtzinger, A., Landschützer, P., Lauvset, S. K., Lefèvre, N., Lienert, S., Liu, J., Marland, G., McGuire, P. C., Melton, J. R., Munro, D. R., Nabel, J. E. M. S., Nakaoka, S.-I., Niwa, Y., Ono, T., Pierrot, D., 560 Poulter, B., Rehder, G., Resplandy, L., Robertson, E., Rödenbeck, C., Rosan, T. M., Schwinger, J., Schwingshackl, C., Séférian, R., Sutton, A. J., Sweeney, C., Tanhua, T., Tans, P. P., Tian, H., Tilbrook, B., Tubiello, F., van der Werf, G., Vuichard, N., Wada, C., Wanninkhof, R., Watson, A., Willis, D., Wiltshire, A. J., Yuan, W., Yue, C., Yue, X., Zaehle, S., and Zeng, J.: Global carbon budget 2021. *Earth Syst. Sci. Data*, 14, 1917–2005. <https://doi.org/10.5194/essd-14-1917-2022>, 2022.
- Galkowski, M., Jordan, A., Rothe, M., Marshall, J., Koch, F.T., Chen, J., Agusti-Panareda, A., Fix, A., and Gerbig, C.: In situ 565 observations of greenhouse gases over Europe during the CoMet 1.0 campaign aboard the HALO aircraft. *Atmos. Meas. Tech.*, 14, 1525–1544. <https://doi.org/10.5194/amt-14-1525-2021>, 2021.
- Gao, Y., Lee, X., Liu, S., Hu, N., Wei, X., Hu, C., Liu, C., Zhang, Z., and Yang, Y.: Spatiotemporal variability of the near-surface CO<sub>2</sub> concentration across an industrial-urban-rural transect, Nanjing, China. *Sci. Total Environ.*, 631–632, 1192–1200. <https://doi.org/10.1016/j.scitotenv.2018.03.126>, 2018.
- 570 Gong, P., Liu, H., Zhang, M., Li, C., Wang, J., Huang, H., Clinton, N., Ji, L., Li, W., Bai, Y., Chen, B., Xu, B., Zhu, Z., Yuan, C., Ping Suen, H., Guo, J., Xu, N., Li, W., Zhao, Y., Yang, J., Yu C., Wang X., Fu H., Yu L., Dronova I., Hui F, Cheng X., Shi X., Xiao F., Liu Q. and Song, L.: Stable classification with limited sample: transferring a 30-m resolution sample set collected in 2015 to mapping 10-m resolution global land cover in 2017. *Sci. Bull.*, 64, 370–373. <https://doi.org/10.1016/j.scib.2019.03.002>, 2019.

- 575 Hajny, K. D., Salmon, O. E., Rudek, J., Lyon, D. R., Stuff, A. A., Stirm, B. H., Kaeser, R., Floerchinger, C. R., Conley, S., Smith, M. L., and Shepson, P. B.: Observations of Methane Emissions from Natural Gas-Fired Power Plants. *Environ. Sci. Technol.*, 53, 8976–8984. <https://doi.org/10.1021/acs.est.9b01875>, 2019.
- Hao, H., Liu, Z. W., Zhao, F. Q., Li, W. Q.: Natural gas as vehicle fuel in China: A review. *Renew. Sust. Energ. Rev.*, 62, 521–533. <https://doi.org/10.1016/j.rser.2016.05.015>, 2016.
- 580 Hartery, S., Commane, R., Lindaas, J., Sweeney, C., Henderson, J., Mountain, M., Steiner, N., McDonald, K., Dinardo, S. J., Miller, C. E., Wofsy, S. C., and Chang, R. Y. W.: Estimating regional-scale methane flux and budgets using CARVE aircraft measurements over Alaska. *Atmos. Chem. Phys.*, 18, 185–202. <https://doi.org/10.5194/acp-18-185-2018>, 2018.
- Herrera, S. A., Diskin, G. S., Harward, C., Sachse, G., De Wekker, S. F. J., Yang, M., Choi, Y., Wisthaler, A., Mallia, D. V., and Pusede, S. E.: Wintertime Nitrous Oxide emissions in the San Joaquin Valley of California estimated from aircraft  
585 observations. *Environ. Sci. Technol.*, 55, 4462–4473. <https://doi.org/10.1021/acs.est.0c08418>, 2021
- Hu, C., Zhang, J., Qi, B., Du, R., Xu, X., Xiong, H., Liu, H., Ai, X., Peng, Y., and Xiao, W.: Global warming will largely increase waste treatment CH<sub>4</sub> emissions in Chinese megacities: insight from the first city-scale CH<sub>4</sub> concentration observation network in Hangzhou, China, *Atmos. Chem. Phys.*, 23, 4501 – 4520, <https://doi.org/10.5194/acp-23-4501-2023>, 2023.
- Hu, N., Liu, S., Gao, Y., Xu, J., Zhang, X., Zhang, Z., and Lee, X.: Large methane emissions from natural gas vehicles in  
590 Chinese cities. *Atmos. Environ.*, 187, 374–380. <https://doi.org/10.1016/j.atmosenv.2018.06.007>, 2018.
- Joo, J., Jeong, S., Shin, J., and Chang, D. Y.: Missing methane emissions from urban sewer networks. *Environ. Pollut.*, 342, 123101. <https://doi.org/10.1016/j.envpol.2023.123101>, 2024.
- Kenea, S. T., Lee, H., Patra, P. K., Li, S., Labzovskii, L. D., Joo, S.: Long-term changes in CH<sub>4</sub> emissions: Comparing  $\Delta\text{CH}_4/\Delta\text{CO}_2$  ratios between observation and proved model in East Asia (2010–2020). *Atmos. Environ.*, 293, 119437.  
595 <https://doi.org/10.1016/j.atmosenv.2022.119437>, 2023.
- Laubach, J., and Fritsch, H.: Convective boundary layer budgets derived from aircraft data. *Agric. For. Meteorol.*, 111, 237–263. [https://doi.org/10.1016/S0168-1923\(02\)00038-2](https://doi.org/10.1016/S0168-1923(02)00038-2), 2002.
- Lee, X.: *Fundamentals of Boundary-Layer Meteorology*. [M]. Springer Cham, 2023.
- Li, S., Kim, S., Lee, H., Kenea, S. T., Kim, J. E., Chung, C. Y., and Kim, Y. H.: Analysis of source distribution of high carbon  
600 monoxide events using airborne and surface observations in Korea. *Atmos. Environ.*, 289, 119316. <https://doi.org/10.1016/j.atmosenv.2022.119316>, 2022.
- Li, Y., Deng, J., Mu, C., Xing, Z., and Du, K.: Vertical distribution of CO<sub>2</sub> in the atmospheric boundary layer: Characteristics and impact of meteorological variables. *Atmos. Environ.*, 91, 110–117. <https://doi.org/10.1016/j.atmosenv.2014.03.067>, 2014.
- Liu, S., Chen, B., Fang, S., Zhang, C., Zang, K., He, W., Chen, Y., Lin, Y., Jin, Z., Chen, Z., Lan, W., and Xu, H.: Contrasting  
605 high-resolution vertical CO<sub>2</sub> patterns: Insights from economically developed regions in southeast China. *J. Geophys. Res. Atmos.*, 130, e2024JD043181. <https://doi.org/10.1029/2024JD043181>, 2025.
- Liu, Y., Zhou, L., Tans, P.P., Zang, K., and Cheng, S.: Ratios of greenhouse gas emissions observed over the Yellow Sea and the East China Sea. *Sci. Total Environ.*, 633, 1022–1031. <https://doi.org/10.1016/j.scitotenv.2018.03.250>, 2018.

- Lloyd, J., Francey, R. J., Mollicone, D., Raupach, M. R., Sogachev, A., Arneth, A., Byers, J. N., Kelliher, F. M., Rebmann, C.,  
610 Valentini, R., Wong, S.-C., Bauer, G., and Schulze, E.-D.: Vertical profiles, boundary layer budgets, and regional flux  
estimates for CO<sub>2</sub> and its <sup>13</sup>C/<sup>12</sup>C ratio and for water vapor above a forest/bog mosaic in central Siberia. *Global  
Biogeochem. Cycles*, 15, 267–284. <https://doi.org/10.1029/1999GB001211>, 2001.
- Machida, T., Ishijima, K., Niwa, Y., Tsuboi, K., Sawa, Y., Matsueda, H., and Sasakawa, M.: Atmospheric CO<sub>2</sub> mole fraction  
data of CONTRAIL-CME, version 2024.1.0, Center for Global Environmental Research, NIES, DOI:10.17595/20180208.001,  
615 2018.
- Narbaud, C., Paris, J. D., Wittig, S., Berchet, A., Saunois, M., Nédélec, P., Belan, B. D., Arshinov, M. Y., Belan, S. B.,  
Davydov, D., Fofonov, A., and Kozlov, A.: Disentangling methane and carbon dioxide sources and transport across the Russian  
Arctic from aircraft measurements. *Atmos. Chem. Phys.*, 23, 2293–2314. <https://doi.org/10.5194/acp-23-2293-2023>, 2023.
- O’Shea, S. J., Allen, G., Gallagher, M. W., Bower, K., Illingworth, S. M., Muller, J. B.A., Jones, B. T., Percival, C.J., Bauguitte,  
620 S. J. B., Cain, M., Warwick, N., Quiquet, A., Skiba, U., Drewer, J., Dinsmore, K., Nisbet, E. G., Lowry, D., Fisher, R.E.,  
France, J. L., Aurela, M., Lohila, A., Hayman, G., George, C., Clark, D. B., Manning, A.J., Friend, A.D., and Pyle, J.: Methane  
and carbon dioxide fluxes and their regional scalability for the European Arctic wetlands during the MAMM project in summer  
2012. *Atmos. Chem. Phys.*, 14, 13159–13174. <https://doi.org/10.5194/acp-14-13159-2014>, 2014.
- Park, Hayoung, Jeong, S., Park, Hoonyoung, Kim, Y., Park, C., Sim, S., Kim, J., Park, J., Kim, H., and Choi, J.: Unexpected  
625 urban methane hotspots captured from aircraft observations. *ACS Earth Sp. Chem.*, 6, 755–765.  
<https://doi.org/10.1021/acsearthspacechem.1c00431>, 2022.
- Ramonet, M., Ciais, P., Nepomniachii, I., Sidorov, K., Neubert, R. E. M., Langendörfer, U., Picard, D., Kazan, V., Biraud, S.,  
Gusti, M., Kolle, O., Schulze, E. D., and Lloyd, J.: Three years of aircraft-based trace gas measurements over the  
Fyodorovskoye southern taiga forest, 300 km north-west of Moscow. *Tellus, Ser. B Chem. Phys. Meteorol.*, 54, 713–734.  
630 <https://doi.org/10.1034/j.1600-0889.2002.01358.x>, 2002.
- Raupach, M. R., Denmead, O. T., and Dunin, F. X.: Challenges in linking atmospheric CO<sub>2</sub> concentrations to fluxes at local  
and regional scales. *Aust. J. Bot.*, 40, 697–716. <https://doi.org/10.1071/BT9920697>, 1992.
- Saito, R., Tanaka, T., Hara, H., Oguma, H., Takamura, T., Kuze, H., and Yokota, T.: Aircraft and ground-based observations  
of boundary layer CO<sub>2</sub> concentration in anticyclonic synoptic condition. *Geophys. Res. Lett.*, 36, L07807.  
635 <https://doi.org/10.1029/2008GL037037>, 2009.
- Sarrat, C., Noilhan, J., Dolman, A. J., Gerbig, C., Ahmadov, R., Tolk, L. F., Meesters, A. G. C. A., Hutjes, R. W. A., Ter Maat,  
H. W., Pérez-Landa, G., and Donier, S.: Atmospheric CO<sub>2</sub> modeling at the regional scale: An intercomparison of 5 meso-scale  
atmospheric models. *Biogeosciences*, 4, 1115–1126. <https://doi.org/10.5194/bg-4-1115-2007>, 2007.
- Satar, E., Berhanu, T. A., Brunner, D., Henne, S., and Leuenberger, M.: Continuous CO<sub>2</sub>/CH<sub>4</sub>/CO measurements (2012–2014)  
640 at Beromünster tall tower station in Switzerland. *Biogeosciences*, 13, 2623–2635, <https://doi.org/10.5194/bg-13-2623-2016>,  
2016.

- Shan, C., Wang, W., Xie, Y., Wu, P., Xu, J., Zeng, X., Zha, L., Zhu, Q., Sun, Y., Hu, Q., Liu, C., and Jones, N.: Observations of atmospheric CO<sub>2</sub> and CO based on in-situ and ground-based remote sensing measurements at Hefei site, China. *Sci. Total Environ.*, 851, 158188. <https://doi.org/10.1016/j.scitotenv.2022.158188>, 2022.
- 645 Shashkov, A., Higuchi, K., and Chan, D.: Aircraft vertical profiling of variation of CO<sub>2</sub> over a Canadian Boreal Forest Site: A role of advection in the changes in the atmospheric boundary layer CO<sub>2</sub> content. *Tellus, Ser. B Chem. Phys. Meteorol.*, 59, 234–243. <https://doi.org/10.1111/j.1600-0889.2006.00237.x>, 2007.
- Shen, S., Yang, D., Xiao, W., Liu, S., and Lee, X.: Constraining anthropogenic CH<sub>4</sub> emissions in Nanjing and the Yangtze River Delta, China, using atmospheric CO<sub>2</sub> and CH<sub>4</sub> mixing ratios. *Adv. Atmos. Sci.*, 31, 1343–1352. <https://doi.org/10.1007/s00376-014-3231-3>, 2014.
- 650 Shibata, Y., Nagasawa, C., Abo, M., Inoue, M., Morino, I., and Uchino, O.: Comparison of CO<sub>2</sub> vertical profiles in the lower troposphere between 1.6 μm differential absorption lidar and aircraft measurements over Tsukuba. *Sensors*, 18, 4064. <https://doi.org/10.3390/s18114064>, 2018.
- Sreenivas, G., Mahesh, P., Biswadip, G., Suresh, S., Rao, P. V. N., Chaitanya, M. K., and Srinivasulu, P.: Spatio-temporal distribution of CO<sub>2</sub> mixing ratio over Bhubaneswar, Varanasi and Jodhpur of India– airborne campaign, 2016. *Atmos. Environ.*, 201, 257–264. <https://doi.org/10.1016/j.atmosenv.2019.01.010>, 2019.
- Sreenivas, G., Mahesh, P., Subin, J., Lakshmi Kanchana, A., Venkata Narasimha Rao, P., and Kumar Dadhwal, V.: Influence of meteorology and interrelationship with greenhouse gases (CO<sub>2</sub> and CH<sub>4</sub>) at a suburban site of India. *Atmos. Chem. Phys.*, 16, 3953–3967. <https://doi.org/10.5194/acp-16-3953-2016>, 2016.
- 660 Stephens, B. B., Gurney, K. R., Tans, P. P., Sweeney, C., Peters, W., Bruhwiler, L., Ciais, P., Ramonet, M., Bousquet, P., Nakazawa, T., Aoki, S., Machida, T., Inoue, G., Vinnichenko, N., Lloyd, J., Jordan, A., Heimann, M., Shibistova, O., Langenfelds, R. L., Steele, L. P., Francey R. J., and Denning, A. S.: Weak northern and strong tropical land carbon uptake from vertical profiles of atmospheric CO<sub>2</sub>. *Science*, 316, 1732–1735. <https://doi.org/10.1126/science.1137004>, 2007.
- Tanaka, T., Miyamoto, Y., Morino, I., MacHida, T., Nagahama, T., Sawa, Y., Matsueda, H., Wunch, D., Kawakami, S., and Uchino, O.: Aircraft measurements of carbon dioxide and methane for the calibration of ground-based high-resolution Fourier Transform Spectrometers and a comparison to GOSAT data measured over Tsukuba and Moshiri. *Atmos. Meas. Tech.*, 5, 2003–2012. <https://doi.org/10.5194/amt-5-2003-2012>, 2012.
- Tiemoko, T. D., Ramonet, M., Yoroba, F., Kouassi, K. B., Kouadio, K., Kazan, V., Kaiser, C., Truong, F., Vuillemin, C., Delmotte, M., Wastine, B., and Ciais, P.: Analysis of the temporal variability of CO<sub>2</sub>, CH<sub>4</sub> and CO concentrations at Lamto, West Africa. *Tellus B: Chem. Phys. Meteorol.*, 73, 1–24. <https://doi.org/10.1080/16000889.2020.1863707>, 2021.
- 670 Tomlin, J. M., Lopez-coto, I., Hajny, K. D., Pitt, J. R., Kaeser, R., Stirm, B. H., Jayarathne, T., Floerchinger, C. R., Commane, R., and Shepson, P. B.: Spatial attribution of aircraft mass balance experiment CO<sub>2</sub> estimations for policy-relevant boundaries: New York City. *Elem. Sci. Anthr.*, 11, 00046. <https://doi.org/10.1525/elementa.2023.00046>, 2023.

- 675 Trousdell, J. F., Conley, S. A., Post, A., and Faloon, I. C.: Observing entrainment mixing, photochemical ozone production, and regional methane emissions by aircraft using a simple mixed-layer framework. *Atmos. Chem. Phys.*, 16, 15433–15450. <https://doi.org/10.5194/acp-16-15433-2016>, 2016.
- Umezawa, T., Matsueda, H., Oda, T., Higuchi, K., Sawa, Y., Machida, T., Niwa, Y., and Maksyutov, S.: Statistical characterization of urban CO<sub>2</sub> emission signals observed by commercial airliner measurements. *Sci. Rep.*, 10, 7963. <https://doi.org/10.1038/s41598-020-64769-9>, 2020.
- 680 Umezawa, T., Niwa, Y., Sawa, Y., Machida, T., and Matsueda, H.: Winter crop CO<sub>2</sub> uptake inferred from CONTRAIL measurements over Delhi, India. *Geophys. Res. Lett.*, 43, 11859–11866. <https://doi.org/10.1002/2016GL070939>, 2016.
- Vilà-Guerau de Arellano, J., Gioli, B., Miglietta, F., Jonker, H. J. J., Baltink, H. K., Hutjes, R. W. A., and Holtslag, A. A. M.: Entrainment process of carbon dioxide in the atmospheric boundary layer. *J. Geophys. Res. Atmos.*, 109, D18110. <https://doi.org/10.1029/2004JD004725>, 2004.
- 685 Vogel, B., Volk, C. M., Wintel, J., Lauther, V., Müller, R., Patra, P. K., Riese, M., Terao, Y., Stroh, F.: Reconstructing high-resolution in-situ vertical carbon dioxide profiles in the sparsely monitored Asian monsoon region. *Commun. Earth Environ.*, 4, 72. <https://doi.org/10.1038/s43247-023-00725-5>, 2023.
- Wang, J., Xiao, W., Hu, N., Li, R., Xu, H., Liu, Y., Bu, L., Chen, L., Liu, Y., Lee, X.: Mobile observations of intracity variations in atmospheric CO<sub>2</sub> and CH<sub>4</sub>. *Adv. Atmos. Sci.*, 43(5), 1033–1047, <https://doi.org/10.1007/s00376-025-5059-4>.
- 690 Watai, T., Machida, T., Ishizaki, N., and Inoue, G.: A lightweight observation system for atmospheric carbon dioxide concentration using a small unmanned aerial vehicle. *J. Atmos. Ocean. Technol.*, 23, 700–710. <https://doi.org/10.1175/JTECH1866.1>, 2006.
- Wratt, D. S., Gimson, N. R., Brailsford, G. W., Lassey, K. R., Bromley, A. M., and Bell, M. J.: Estimating regional methane emissions from agriculture using aircraft measurements of concentration profiles. *Atmos. Environ.*, 35, 497–508. [https://doi.org/10.1016/S1352-2310\(00\)00336-8](https://doi.org/10.1016/S1352-2310(00)00336-8), 2001.
- 695 Xueref-Remy, I., Messenger, C., Filippi, D., Pastel, M., Nedelec, P., Ramonet, M., Paris, J. D., and Ciais, P.: Variability and budget of CO<sub>2</sub> in Europe: Analysis of the CAATER airborne campaigns-Part 1: Observed variability. *Atmos. Chem. Phys.*, 11, 5655–5672. <https://doi.org/10.5194/acp-11-5655-2011>, 2011.

## Web References

- 700 Effectiveness of the Work in Comprehensively Promoting the Construction of Beautiful Nanjing. Retrieved from [https://www.nanjing.gov.cn/zt/qmtjmlnjjs/gzcx/202408/t20240822\\_4747015.html](https://www.nanjing.gov.cn/zt/qmtjmlnjjs/gzcx/202408/t20240822_4747015.html). Accessed August 15, 2025.
- Work Summary of Beijing Municipal Bureau of Landscape and Forestry for 2023. Retrieved from [https://yllhj.beijing.gov.cn/zwgk/sx/202401/t20240108\\_3528516.shtml](https://yllhj.beijing.gov.cn/zwgk/sx/202401/t20240108_3528516.shtml). Accessed August 15, 2025.
- China's Energy Transition. Retrieved from [https://www.gov.cn/zhengce/202408/content\\_6971115.htm](https://www.gov.cn/zhengce/202408/content_6971115.htm). Accessed January 31, 2026.
- 705